Int. J. Environ. Sci. Technol. (2016) 13:1137–1148
DOI 10.1007/s13762-016-0955-x

ORIGINAL PAPER

Synthesis of Fe_3O_4-loaded porous carbons developed from rice husk for removal of arsenate from aqueous solution

S. Luo[1] · M.-N. Shen[2] · F. Wang[1] · Q.-R. Zeng[1] · J.-H. Shao[1] · J.-D. Gu[1,3]

Received: 23 March 2015 / Revised: 16 December 2015 / Accepted: 9 February 2016 / Published online: 24 February 2016

Abstract A simple one-step synthetic approach using rice husk has been developed to prepare magnetic Fe_3O_4-loaded porous carbons composite (MRH) for removal of arsenate (As(V)). The characteristics of adsorbent were evaluated by transmission electron microscope, scanning electron microscopy, X-ray diffraction, Fourier transform infrared spectroscopy, Brunauer–Emmett–Teller analysis, and thermogravimetric analysis. On account of the combined advantages of rice husk carbons and Fe_3O_4 nanoparticles, the synthesized MRH composites showed excellent adsorption efficiency for aqueous As(V). The removal of As(V) by the MRH was studied as a function of contact time, initial concentration of As(V), and media pH. The adsorption kinetics of As(V) exhibited a rapid sorption dynamics by a pseudo-second-order kinetic model, implying the mechanism of chemisorption. The adsorption data of As(V) were fitted well to the Langmuir isotherm model, and the maximum uptake amount (q_m) was calculated as 4.33 mg g^{-1}. The successive regeneration and reuse studies showed that the MRH kept the sorption efficiencies over five cycles. The obtained results demonstrate that the MRH can be utilized as an efficient and low-cost adsorbent for removal of As(V) from aqueous solutions.

Keywords Adsorption · Carbon · Characterization · Langmuir · Magnetic material

Introduction

Due to the high specific surface area, porosity, thermal stability, and chemical inertness, porous carbon (PC) has shown significant application as adsorbent/catalytic support for air and water pollution control (Choi et al. 2008; Pereira et al. 2003). However, large-scale utilization of PC has been limited because of problems such as high cost, difficult separation, and dispersion (Ai and Jiang 2010).

Over the last decade, carbonaceous materials prepared from agricultural waste biomass have gained increasing attention because they are renewable, are highly abundant, and have low cost. This is an effective way to reduce the production cost of PC. In addition, the transformation of biomass to carbonaceous materials is beneficial for sequestering carbon from biomass resources, and it consequently efficiently reduces CO_2 emissions (Liu and Zhang 2010). A survey of literature indicated that various agricultural waste biomass, such as rice straws (Yun et al. 2001), oil palm (Foo and Hameed 2009), cornstalks (Zhang et al. 2008), olive waste, sugar cane bagasse, and wheat straw (Zanzi et al. 2001), have been used as substrates for PC production.

Electronic supplementary material The online version of this article (doi:10.1007/s13762-016-0955-x) contains supplementary material, which is available to authorized users.

✉ S. Luo
rose850101@163.com

[1] College of Resources and Environment, Hunan Agricultural University, Changsha 410128, People's Republic of China

[2] Key Laboratory of Songliao Aquatic Environment, Ministry of Education, Jilin Jianzhu University, Changchun 130118, People's Republic of China

[3] Laboratory of Environmental Microbiology and Toxicology, School of Biological Sciences, The University of Hong Kong, Pokfulam Road, Pok Fu Lam, Hong Kong SAR, People's Republic of China

Rice husks, a by-product of rice milling, is one of the largest agricultural wastes. The dry rice husk consists of 70–85 % organic matter and the remaining consists of silica (Fang et al. 2004; Patel et al. 1987), which makes it a good precursor for PC. Unfortunately, the untreated rice husk carbon was ineffective for the removal of inorganic/organic contaminants. By modifying the adsorbing properties of rice husk, its efficiency as a PC material can be significantly improved. The high efficiency of prepared PC-supported iron or iron oxide composites has been confirmed in the adsorption and catalytic degradation of pollutant in air and wastewater (Dang et al. 2009; Yang et al. 2008; Zhang et al. 2007).

In order to solve the separation problem of PC, many researchers have proposed the synthesis of magnetically separable PC (Zhang et al. 2007; Zhang et al. 2011), which would greatly simplify the separation process. Additionally, the presence of Fe_3O_4 particles results in the chemical stability and low toxicity of PC, which is essential for widespread utilization of this method for pollutant treatment in groundwater and wastewater (Kakavandi et al. 2013). Therefore, a combination between rice husk-based PC (RHC) and Fe_3O_4 nanoparticles can create a promising adsorbent with high adsorption capacities and easy recovery from the aquatic system. The preparation of Fe_3O_4-loaded PC is generally carried out via several tedious, consecutive steps including carbon material fabrication, PC oxidation, and iron precursor impregnation (Chen et al. 2007).

In this study, a simple and one-step synthetic approach for fabricating magnetic Fe_3O_4-loaded PC composites from rice husks (MRH) was developed by impregnating the magnetic precursor into the rice husk followed by thermochemical conversion. The as-prepared MRH was characterized via transmission electron microscopy (TEM), scanning electron microscopy (SEM), X-ray diffraction (XRD), Fourier transform infrared (FTIR) spectroscopy, Brunauer–Emmett–Teller (BET) analysis, and thermogravimetric analysis (TGA). Arsenate (As(V)) was selected as model pollutant to test the ion adsorption capacity of MRH. The effect of the media pH on As(V) adsorption was evaluated as well as adsorption kinetics, isotherms, and regeneration efficiency of the materials. The information can be applied for both designing low-cost and easily available adsorption material based on rice husk PC for further practical applications in As(V)-contaminated wastewater treatment. This research was carried out from June 2013 to November 2014 at Hunan Agricultural University and Jilin Jianzhu University.

Materials and methods

Materials

Ferric chloride hexahydrate ($FeCl_3 \bullet 6H_2O$), analytical-grade ethanol, and Na_2HAsO_4 were supplied by Sinopharm Chemical Reagent Co., Ltd, China. Rice husk was obtained from a rice milling factory in Changsha suburb. All chemicals were analytical grade or higher and were used for further treatment.

Preparation of MRH and RHC

The rice husk was firstly washed and dried at 105 °C for 24 h and ground into dimensions ≤80 meshes after being air-cooled. Two grams of the drying rice husk was immersed into 20 ml of $FeCl_3$ solution (1 mol L^{-1}) with using an ultrasonic bath for 2 h at room temperature and then stirred at 60 °C for 12 h. Subsequently, the mixture was separated by filtration and dried at 80 °C for 2 h. After ground, the sample was heated to 800 °C with heating rate 10 °C min^{-1} under 30 mL min^{-1} N_2 flow and hold at 800 °C for 60 min. Finally, the product was cooled inside the furnace under N_2 atmosphere to get MRH. For comparison, the rice husk without $FeCl_3$ impregnation was pyrolyzed under the same procedure at 800 °C. The product obtained was designated as RHC.

Characterization

Some physical properties of MRH were measured. XRD analysis (Switzerland ARL X'TRA, $\lambda = 1.5418$ Å) was conducted to determine the crystal structure and crystallinity of the MRH composites. The BET surface areas were determined from nitrogen adsorption isotherm via a JW-04 surface analyzer. The pore size distribution of MRH was derived from the desorption branch of the isotherm based on the Barrett–Joyner–Halenda model, and the total pore volume was measured from the amount of the nitrogen adsorbed at P/P_0 ca. 0.99. The surface physical morphology, porosity, shape, and size of the composites were examined by SEM (JEOL, JSM-6380LV) and TEM (JEOL, JEM-1230). FTIR analysis was performed using a NEXUS870 (Thermo Nicolet) FTIR spectrometer in the wave number range of 400–4000 cm^{-1}. The bulk chemical compositions of RHC and MRH were measured by XRF spectrometry (Switzerland ARL Corporation). TGA was carried out by a TA Instruments Q5000IR analyzer (USA) over the temperature range 50–775 °C at a heating rate of 10 °C min^{-1} under nitrogen atmosphere. The zeta potential

of MRH particles were measured at various pH with a DELSA 440SX (USA). Magnetization curve of samples was measured by a HH-15 vibrating sample magnetometer (VSM, Nanjing, China) at room temperature.

Adsorption experiments

As(V) solutions were prepared by dissolving Na_2HAsO_4 in de-ionized water to yield a 1000 mg L^{-1} stock. For each adsorption experiment, 0.2 g of MRH was added into a 150-mL glass bottle containing 100 mL As(V) solution. The bottles were placed on the rotary shaker for 100 min at 200 rpm and 25 ± 2 °C. Samples were withdrawn with a 5-mL syringe at regular intervals, filtered through a 0.45-μm membrane filter, and the filtrate was preserved with 6 N HNO_3 and stored at 4 °C for further analysis.

Equilibrium adsorption isotherms were investigated with the initial As(V) concentrations from 1 mg L^{-1} to 10 mg L^{-1} and MRH dosage was 2 g L^{-1}. The effect of initial pH (3–11) on the As(V) adsorption were also studied. The solutions pH was adjusted initially using 0.1 M HCl or NaOH. All the adsorption experiments were performed in triplicate. The initial As(V) concentrations and residual after adsorption were determined by Inductively Coupled Plasma Optical Emission Spectroscopy (ICP-OES) at 189.042 nm. A 1.0 mg L^{-1} As(V) solution for instrument performance check was measured after every five samples. A 10 % variation would interrupt the analysis, and the ICP would be programmed to recalibrate the As(V) determination method. Calibration blank solution was measured after samples to minimize the carryover effect. Following this procedure, the detection limit of arsenic was 20 μg L^{-1}.

Regeneration and reuse of MRH

To test the reusability of composites, the spent MRH were separated from the solutions by an external magnet and then brought into contact with 0.1 M NaOH solution. The mixture was stirred (150 rpm) for 6 h at 25 ± 2 °C. After regeneration, MRH were rinsed with de-ionized water for three times and resuspended in a fresh As(V) solution for the subsequent adsorption. Five cycles of consecutive adsorption–desorption experiments were carried out.

Results and discussion

Characterization of the composites

XRD and XRF analysis

To investigate the transformation of the iron oxides by carbon support, the MRH composites were thermally treated under the same procedure at 600, 700, and 800 °C. The XRD patterns of samples are illustrated in Fig. 1. The samples MRH (600) and MRH (700) exhibited a weak peak at 30.3° attributed to peak of carbon (JCPDS file No. 1-640), but this diffraction peak disappeared in the XRD pattern of MRH (800), indicating the amorphous phase of the carbon. The characteristic diffraction peaks at 33.2°, 35.7°, 43.2°, 52.6°, 54.1°, 62.5°, and 74.8° corresponding to (220), (311), (400), (422), (511), (440), and (533) reflections, respectively, were well indexed to the face-centered-cubic-structured magnetite Fe_3O_4 (JCPDS file No. 19-0629) (Sun et al. 2011). The average crystallite size of Fe_3O_4 nanoparticles calculated by using the Debye–Scherrer equation was about 24.5 nm (Patterson 1939). At the same time, several diffraction peaks of Fe_3O_4 were also clearly observed on MRH (600) and MRH (700). However, the peaks for hematite obviously decreased after treatment at 800 °C with simultaneous increase in the characteristic reflection magnetite and/or maghemite. All the samples exhibit a set of diffraction peaks can be indexed to SiO_2 (JCPDF file NO. 82-0512). Considering the total iron chemical analysis and the reduction process with rice husk pyrolysis, it was suggested that the iron oxide in the MRH (800) was mainly in the form of Fe_3O_4. Furthermore, the reduction process was more efficient when the composite was heated at 800 °C, which was chosen as a model in the following experiments.

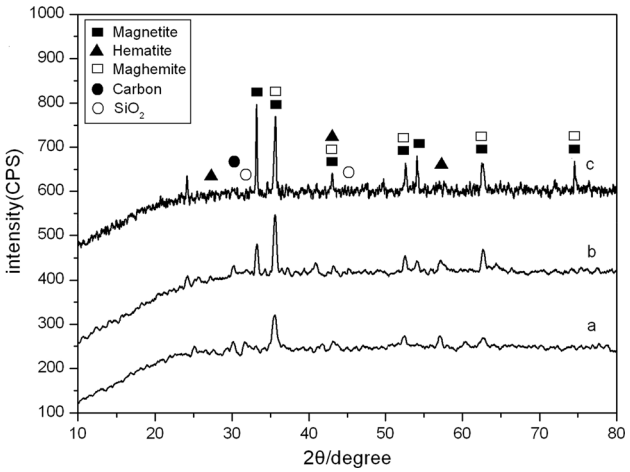

Fig. 1 XRD patterns of the MRH composites heated at different temperature. (*a*) MRH (600), (*b*) MRH (700), (*c*) MRH (800)

The chemical compositions of the samples were determined by XRF, and the data are listed in Table SM 1. The content of iron in MRH reached 73.32 % (w/w), whereas it was only 2.39 % (w/w) in RHC. Fe_3O_4 was introduced into the structure of porous carbon successfully.

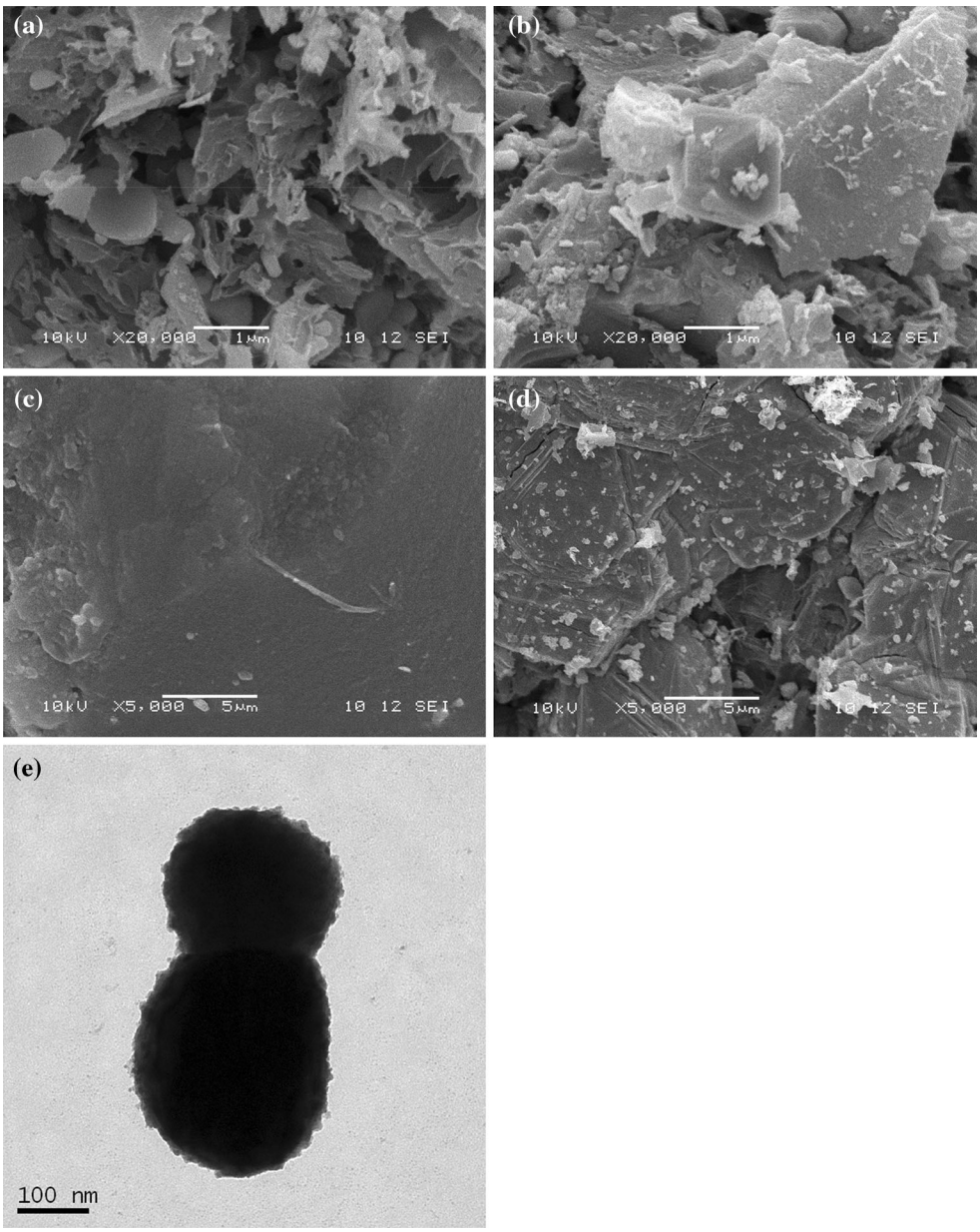

Fig. 2 SEM images of RHC (**a**, **c**) and MRH (**b**, **d**) samples and TEM image of MRH (**e**)

Morphology studies

According to the SEM images, pores with different size and form were distributed on the external surface of RHC and MRH (Fig. 2a, b). Unlike smooth and homogeneous surface of RHC, the surface of MRH was much coarser due to the deposition of the Fe_3O_4 nanoparticles (Fig. 2c, d). The nubbly substance was rice husk-based porous carbon, while the brighter and small aggregate form was the Fe_3O_4, which was adhered on PC. The crystals of iron oxides on the surface of MRH can also be clearly identified by the TEM image in Fig. 2e (protrusions on the PC surface are Fe_3O_4). In addition, the average diameter of Fe_3O_4 nanoparticles was estimated to be about 20 nm, which was close to the result obtained from XRD. Obviously, the uneven surface of MRH resulted in the increased adsorption active sites and created a beneficial condition for attracting more arsenate around the adsorbents and

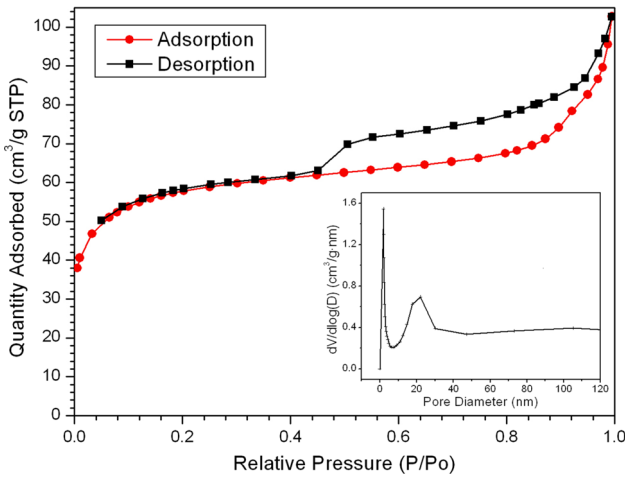

Fig. 3 Nitrogen adsorption–desorption isotherms and pore size distributions (*inset*) of MRH composites

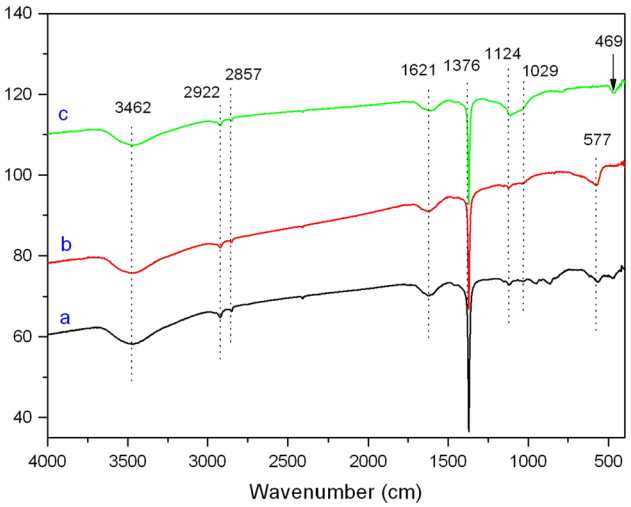

Fig. 4 FTIR spectra of the (*a*) MRH, (*b*) Fe_3O_4, and (*c*) RHC

correspondingly enhanced the adsorption efficiency and capacity (Zhu et al. 2011).

Surface area and pore properties

Textural parameters of MRH and RHC are presented in Table SM 2. The BET surface area of the MRH composites was detected to be 269.43 $m^2\ g^{-1}$, which was smaller than that of the non-magnetic RHC (384.18 $m^2\ g^{-1}$). It is indicated that the formation of Fe_3O_4 nanoparticles contributed to a reduction in BET surface area and pore volume, but also reflected an increase in the average pore diameter. This might be due to the presence of Fe_3O_4 nanoparticles which blocked and occupied the pores structure of carbon. Previous studies have reported that the oxidation action of ferric salt played a role as an activating agent for carbon materials (Castro et al. 2010; Do et al. 2011; Oliveria et al. 2009). However, the activation is not sufficient to cover the lost part of the porosity attributed to the present of Fe_3O_4 nanoparticles. Figure 3 shows the N_2 adsorption–desorption isotherms and the pore size distribution (inset) obtained for MRH sample. The adsorption isotherms exhibit a combined feature of type II and IV curves, suggesting the formation of mesopores in absorbent. Furthermore, the hysteresis loop of H3 exhibiting non-limiting adsorption at high relative pressure implied the slit-shaped porosity of MRH (Sing 1985).

According to the classification of IUPAC pore dimensions, the pores of absorbents can be divided into three types, i.e., micropores ($d < 2$ nm), mesopores (2 nm $< d <$ 50 nm), and macropores ($d > 50$ nm) (Kamari et al. 2009). The pore diameter distributions of MRH (Fig. 3 inset) show that a vast majority of the pores fall into the range of mesopores (between 2 and 22 nm). In addition, the total pore volume of the MRH was 0.134 $cm^3\ g^{-1}$.

FTIR analysis

To qualitatively identify the groups on MRH, Fe_3O_4, and RHC surface, the FTIR spectra was analyzed, as Fig. 4 shows. In all the spectra, there were seven consistent absorption regions at 3462, 2922, 2857, 1621, 1376, 1124, and 1029 cm^{-1}. A wide band located around 3462 cm^{-1} was attributed to hydroxyl groups or chemisorbed water (Stuart et al. 1996). The weak peaks appeared at 2922 and 2857 cm^{-1} can be assigned to C–H stretching vibration, while the absorbance band at 1621 cm^{-1} corresponds to vibration of the C=O. The peaks at 1376, 1124, and 1029 cm^{-1} were all assigned to oxygen functionalities such as carboxylate moieties, highly conjugated C–O stretching, and C–O stretching in carboxylic groups (Moreno-Castilla et al. 1997). In the curves a and c, bands at 460–480 cm^{-1} were probably caused by the Si atom attached initially to the O in the rice husk (Liou 2004). The band at 577 cm^{-1} (curves a and b) was assigned to Fe–O stretching vibration and torsional vibration of Fe_3O_4. In addition, the characteristic adsorption around 630 cm^{-1} was not observed, implying the absence of the γ-Fe_2O_3 in MRH (Namduri and Nasrazadani 2008).

TGA analysis

The TGA curve of MRH composites (Fig. SM 1) was characterized by two different temperature stages. An

initial mass loss over the range from 39.52 to 78.27 °C was about 3.436 % due to the loss of residual water in the sample. About 13.63 % of mass loss occurs in the 292.04–548.13 °C transition period as a result of the further thermal decomposition of the organic substances (Liou and Wu 2009). The residual weight for MRH was 84.8 wt %, which was larger than the common porous carbon materials, indicating that Fe_3O_4 nanoparticles were embedded in MRH. This was in agreement with the results of XRD and SEM analysis.

Magnetic properties

Figure SM 2 shows the magnetization curves of MRH obtained by VSM at room temperature. From the plot of magnetization (M) and magnetic field (H) and its enlargement near the origin, the weak hysteresis indicated the magnetic composite was almost superparamagnetic. It was suggested that small and uniform Fe_3O_4 nanoparticles were presented in MRH. The saturation magnetization (M_s) of synthesized MRH was found to be 3.46 emu g^{-1}, which was lower than the bare Fe_3O_4 particles ($M_s = 58.94$ emu g^{-1}) (Yang et al. 2005). The decrease was mainly attributed to the existence of the non-magnetic PC and the nanoscale of magnetic particles. As displayed in Fig. SM 2 inset, after dispersion of MRH in water, they could be easily and quickly separated from suspension by an external magnetic field. It is confirmed that MRH can be utilized as a magnetic materials to collect pollutants from liquid phase, which is very important in water treatment application.

Adsorption of As(V) from aqueous solutions

Effect of pH on the adsorption of As(V)

The pH is an important factor in the application of metal-modified adsorbents for arsenic removal, which directly influence the charge state on the adsorbent surface and the arsenate species in aqueous solution (Dang et al. 2009; Liu et al. 2010). So the effect of pH on the adsorption of As(V) (5 mg L^{-1}) was investigated using reaction solution in the pH range of 3–11. From Fig. 5, the efficiency of arsenate removal was strongly dependent on media pH. A gradual growth of the As(V) adsorption capacity could be seen as the pH value increased from 3 to 7, with a maximums at the pH 7. As the pH value was further increased, the As(V) adsorption decreased dramatically after pH 7. In order to diminish the influence of pH and keep adsorption conditions close to natural environments, the pH in following tests was controlled at 7 ± 0.1 using bicarbonate buffer solution. The similar result was obtained in previous work by Liu et al. (2010) for the adsorption of As(V) by MY (Fe_3O_4-loaded activated carbon), where pH 8.0 appears to be the optimum pH.

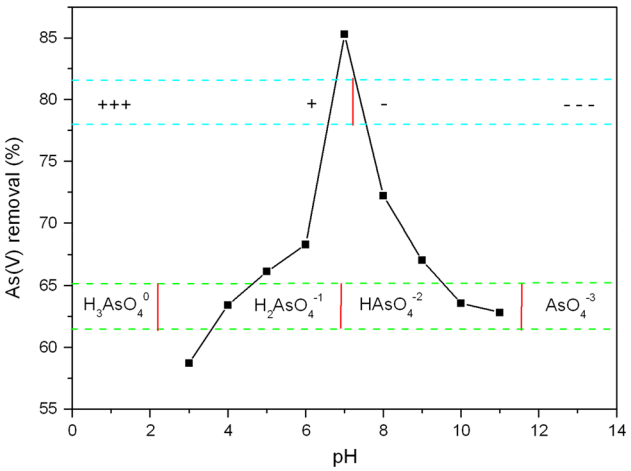

Fig. 5 Effect of initial pH on the As(V) adsorption on MRH. C_0, 5.0 mg L^{-1}; MRH dosage, 2 g L^{-1}; agitation rate, 200 rpm; T, 25 ± 2 °C; contact time, 60 min

The pH-dependent behavior of As(V) removal by MRH could be ascribed mainly to both affinity adsorption and chemical reaction with Fe_3O_4, which occur depending on the MRH properties and the arsenate speciation. On account of the several components in the MRH system (carbon, silica, Fe_3O_4, etc.), the affinity adsorption and chemical reaction might occur simultaneously (Dang et al. 2009; Zhang and Itoh 2005).

The propensity of ionization can be expressed by the dissociation constant (pK_a). For arsenate, pK_a values are $pK_{a1} = 2.19$, $pK_{a2} = 6.94$, and $pK_{a3} = 11.5$ (Bard et al. 1985). The major arsenate species in different pH range are also presented in Fig. 5, which varied from H_3AsO_4, $H_2AsO_4^-$, $HAsO_4^{2-}$, to AsO_4^{3-} when the pH changed from acidic mediums to alkaline mediums. At the pH range studied (3–11), arsenate exists as the oxy-anions $H_2AsO_4^-$ and $HAsO_4^{2-}$ in the aqueous solution. pH_{ZPC} is the pH of zero point charge of the adsorbents. The pH_{ZPC} of the synthesized MRH was determined to be pH 7.2, above which the surface was negatively charged and the attraction between arsenate and MRH became weaker and then changed to repulsion (Chang et al. 2010). Hence, the As(V) adsorption capacity reduced obviously with increasing pH, and this has been reported in previous studies (Chang et al. 2010; Chen et al. 2007; Liu et al. 2010; Zhang and Itoh 2005).

It was suggested that aqueous arsenate species have no direct relationship with the surface arsenate species adsorbed on the absorbent surfaces (Jia et al. 2007). Before complexing with the MRH surface in neutral to alkaline region (pH 7, 8), the aqueous arsenate species ($H_2AsO_4^-$) underwent a dissociation/deprotonation process, forming as $HAsO_4^{2-}$ and AsO_4^{3-} (Bard et al. 1985). At pH < 7, the adsorption of arsenate was greatly influenced by the deprotonation of $H_2AsO_4^-$. As pH increased from 3 to 7, the deprotonation process of $H_2AsO_4^-$ was promoted and the electrostatic attraction became greater, as a result adsorption was enhanced. The results demonstrated that the MRH synthesized in this work can be employed as good adsorbents to treat arsenate polluted wastewater under neutral condition.

Adsorption kinetics

Adsorption kinetics is an important characteristic describing the efficiency of an adsorbent. It determines the adsorbate uptake rate and the residence time taken to reach adsorption equilibrium at the solid–solution interface. Adsorption kinetics can be controlled by several factors, such as the physical or chemical characteristics of the adsorbent and the operating conditions (Dang et al. 2009). The adsorption capacity was studied in As(V) aqueous solution with different initial concentrations (2, 5, 10 mg L^{-1}) with time from 2 to 100 min. In Fig. 6a, the kinetic appears to consist of two stages, an initial stage in which the adsorption was quite fast and a second stage in which the uptake process was much slower and gradually

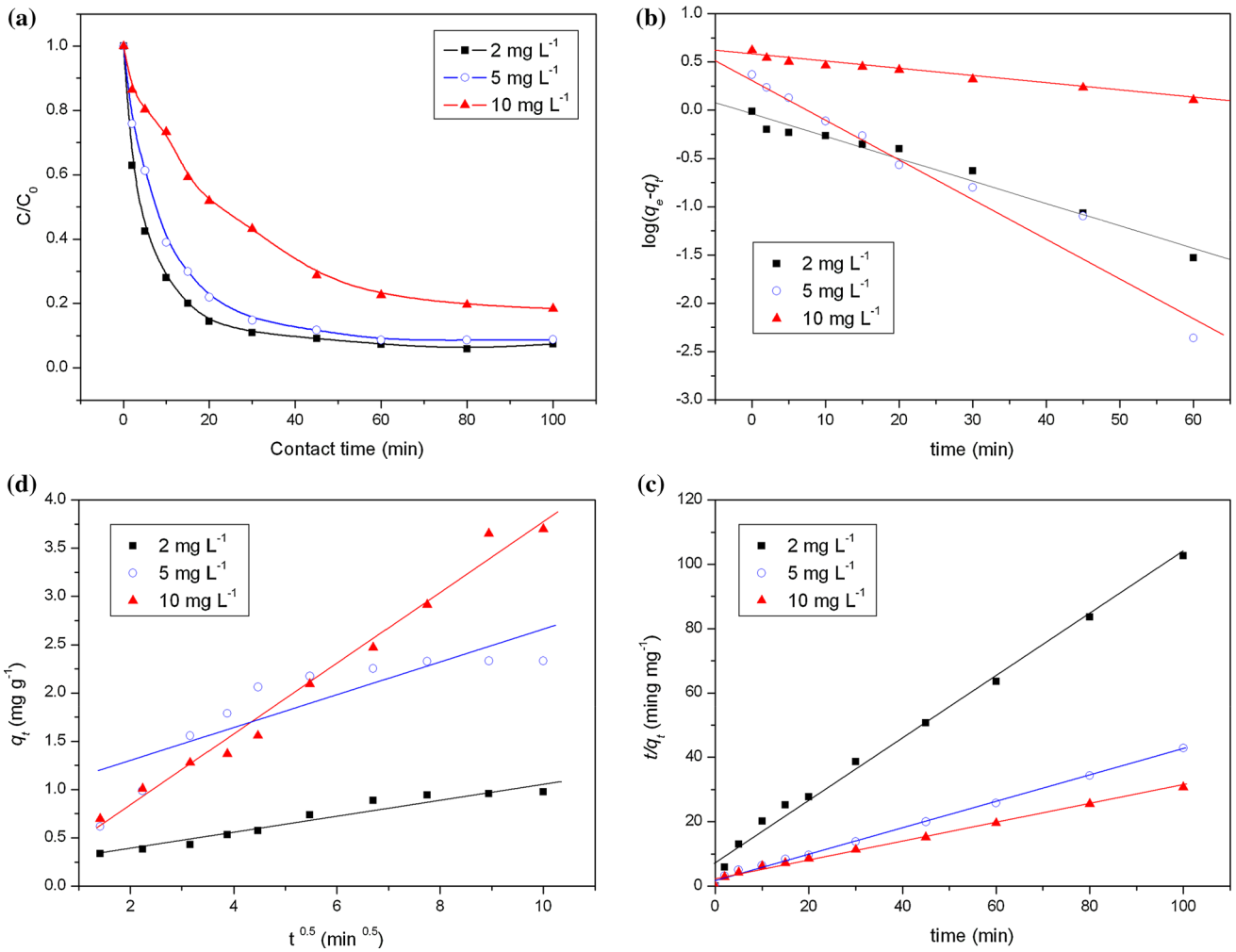

Fig. 6 **a** Relationship of As(V) concentration versus time for initial concentrations of 2.0, 5.0, 10.0 mg L^{-1} As(V) removal by MRH; linear regressions of kinetic plots: **a** Lagergren pseudo-first-order model, **b** pseudo-second-order model, and **c** Weber and Morris intraparticle diffusion model. MRH dosage, 2 g L^{-1}; natural pH; agitation rate, 200 rpm; T, 25 ± 2 °C

reached equilibrium. The high rate of As(V) uptake may come from the greater availability of binding sites on the adsorbent at the initial stage of adsorption. But along with the reaction, the surface of MRH was exhausted; adsorption slowed down and finally reached equilibrium.

In order to investigate the controlling mechanism of adsorption processes such as transfer and chemical reaction, Lagergren pseudo-first-order [Eq. (1)] (Lagergren 1898), pseudo-second-order [Eq. (2)] (Ho and McKay 1999), and Weber and Morris intra-particle diffusion models [Eq. (3)] (Weber and Morris 1963) were employed to study the kinetics of As(V) adsorption by MRH.

$$\log(q_e - q_t) = \log\ q_e - \frac{k_1 t}{2.303} \quad (1)$$

$$\frac{t}{q_t} = \frac{1}{k_2 q_e^2} + \frac{t}{q_e} \quad (2)$$

$$q_t = k_i t^{0.5} + c \quad (3)$$

where q_e and q_t are the adsorption amounts of As(V) (mg g^{-1}) at equilibrium and time t (min), respectively; k_1 (min^{-1}), k_2 (g mg^{-1} min^{-1}), and k_i (mg g^{-1} $min^{-0.5}$) are the rate constants of pseudo-first-order and pseudo-second-order adsorption. Values of k_1 and q_e can be determined from the plots of $\log(q_e - q_t)$ against t for Eq. (1). The slope and intercept of the linear plots of t/q_t versus t yields the values of $1/q_e$ and $1/k_2 q_e^2$ for Eq. (2). Further, c (mg g^{-1}) and intra-particle diffusion rate constant (k_i) can be calculated from the slop of the linear plots of q_t versus $t^{0.5}$ for Eq. (3).

The kinetics parameters were determined at different initial As(V) concentrations and the results are presented in Fig. 6b, c and Table 1. Only initial kinetic data (up to 60 min) have been used for modeling with Lagergren pseudo-first-order model. The calculated values [$q_{e(cal)}$] obtained from the pseudo-first-order kinetic model did not agree with the experimental values [$q_{e(exp)}$], which revealed that the adsorption process of As(V) on MRH was not fit to the Lagergren pseudo-first-order adsorption expression. However, the $q_{e(exp)}$ values were close to those derived from the pseudo-second-order kinetics model for different initial As(V) concentrations. The values of correlation coefficient (R^2) for the pseudo-second-order model were >0.99 for all As(V) concentrations. At the same time, the constants of the Weber and Morris intra-particle diffusion models for the same experimental data were obtained from the plot of q_t against $t^{0.5}$ (Table 1). k_i increases as the initial As(V) concentration increase; it is because k_i is directly related to q_e and intra-particle diffusivity. If the regression of q_t versus $t^{0.5}$ is linear and passes through the origin, then intra-particle diffusion is the sole rate-limiting step (Kannan and Sundaram 2001). However, these lines do not pass through the origin. The correlation coefficients between 0.755 and 0.980 for all the cases suggested that the intra-particle diffusion model could not used to describe the adsorption. These observations revealed that the rate-limiting step might be chemical adsorption or chemisorption involving valence forces through sharing or exchange of electrons between As(V) and MRH (Ho 2006). According to previous studies, the adsorption of arsenic on other iron-modified materials, such as CTAB-modified Fe_3O_4, magnetite-reduced graphene oxide, and iron-modified rice husk carbon, also followed the pseudo-second-order model (Dang et al. 2009; Chandra et al. 2010).

Adsorption isotherms

As shown in Fig. 7, the uptake amount of As(V) for MRH, Fe_3O_4, or RHC after 60 min varied according to the equilibrium concentrations of As(V). The insert is the adsorption by Fe_3O_4 or RHC. The adsorption of As(V) for MRH increased with increase in the initial concentrations from 1 to 8 mg L^{-1} and then remained stable with a further increase in concentration of As(V). This may be due to the finite adsorption sites at a fixed dose of MRH and the saturation of adsorbent surface. At all initial As(V) concentrations (1–10 mg L^{-1}), MRH had higher As(V) adsorption capacity than Fe_3O_4 or RHC at the same conditions. It was mainly caused by the incorporation of the Fe_3O_4 nanoparticles in the

Table 1 Kinetic parameters of different models and experimental q_e values for As(V) adsorption

C_0 (mg L^{-1})	$q_{e(exp)}$ (mg g^{-1})	Lagergren pseudo-first-order model			Pseudo-second-order model			Intra-particle diffusion model		
		$q_{e(cal)}$ (mg g^{-1})	k_1 (min^{-1})	R^2	$q_{e(cal)}$ (mg g^{-1})	k_2 (g mg^{-1} min^{-1})	R^2	c	k_i (mg g^{-1} $min^{-1/2}$)	R^2
2	0.97	0.92	0.05343	0.972	0.99	0.1506	0.991	0.22	0.0853	0.946
5	2.33	2.21	0.03927	0.959	2.39	0.09977	0.997	0.85	0.1838	0.755
10	4.09	3.69	0.01773	0.976	4.03	0.02434	0.992	0.49	0.3772	0.980

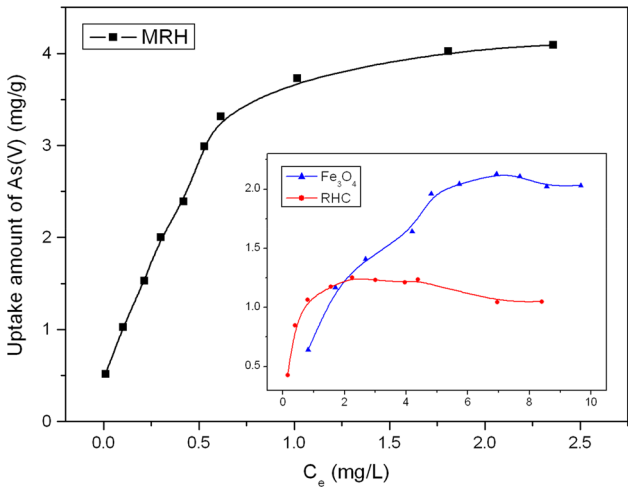

Fig. 7 Variation of the equilibrium liquid concentration of As(V) in solutions with uptake amount of As(V) on different adsorbents (insert represents uptake of As(V) by Fe_3O_4 and RHC individually). MRH or RHC dosage, 2 g L^{-1}; Fe_3O_4 dosage, 0.2 g L^{-1}; natural pH; agitation rate, 200 rpm; T, 25 ± 2 °C; contact time, 60 min

rice husk carbons and the changed physical and chemical characteristics of adsorbent.

The distribution of As(V) between the solid phase and the liquid phase at adsorption equilibrium could be described based on the adsorption isotherm. In this study, the adsorption data were analyzed according to the two well-known Langmuir (1918) and Freundlich (1906) isotherm models, expressed as Eq. (4) and (5), respectively.

$$\frac{C_e}{q_e} = \frac{1}{q_m K_L} + \frac{C_e}{q_m} \tag{4}$$

$$q_e = K_F C_e^{1/n} \tag{5}$$

where C_e is the concentration of As(V) (mg L^{-1}) at equilibrium, q_e is the amount of As(V) adsorbed per unit weight of MRH at equilibrium (mg g^{-1}), and q_m and K_L are Langmuir constants related to the maximum adsorption capacity (mg g^{-1}) and the energy of adsorption (L mg^{-1}), respectively. K_F (L g^{-1}) is the Freundlich constant, and n (dimensionless) is the indicator of isotherm nonlinearity related to the heterogeneity of sorption sites.

The theoretical parameters of adsorption isotherms along with regression coefficients (R^2) are summarized in Table 2. The isothermal characteristics has shown that As(V) removal by MRH was in high accordance with Langmuir isotherm ($R^2 > 0.99$), while the Freundlich isotherm ($R^2 = 0.943$) was not as adequate as Langmuir isotherm. It means that adsorption of As(V) on MRH is the complete monolayer adsorption rather than non-ideal adsorption on heterogeneous surfaces and multilayer adsorption. This observation indicated that the distribution of active sites onto MRH surface is homogenous, and a

Table 2 Isotherm parameters for the As(V) adsorption onto MRH

	Langmuir isotherm constants			Freundlich isotherm constants		
	q_m (mg g^{-1})	K_L (L mg^{-1})	R^2	K_F (L g^{-1})	n	R^2
MRH	4.33	3.91	0.990	0.06197	0.4274	0.944

high Langmuir constant ($K_L = 3.91$) implied strong affinity of As(V) to the MRH surface under the experimental conditions. In addition, the calculated value of q_m obtained form Langmuir plots was consistent with the experimental obtained.

A further analysis of the characteristics of the Langmuir isotherm model can be explained in terms of a dimensionless constant separation factor for equilibrium parameter R_L. It is determined by the following equation:

$$R_L = \frac{1}{1 + K_L C_0} \tag{6}$$

where K_L is the Langmuir constant (L mg^{-1}) and C_0 is the initial As(V) concentration (mg L^{-1}). The feasibility of the reactions are explained using the value of R_L ($R_L > 1$—unfavorable, $R_L = 1$—linear, $1 > R_L > 0$—favorable, $R_L = 0$—irreversible). The values of R_L were found in the range of 0.02–0.20, confirming that the adsorption is favorable. However, the actual adsorption mechanism of MRH might be complex, including surface complexation, electrostatic attraction, and ion exchange.

Comparison with other adsorbents

Many adsorbents have been synthesized for arsenate removal from water. The comparison of the adsorption capacity of MRH with other adsorbents examined for the removal of As(V) reported in the literature is summarized in Table SM 3. The value of MRH for As(V) is reliable compared to that of corresponding adsorbents, which is much higher than Fe_3O_4 and RHC in this study, nanoiron (hydr)oxide-impregnated GAC, Fe-GACs, and iron oxide-coated cement. The adsorption capacity of MRH is lower when compared with iron-containing ordered mesoporous carbon, iron-impregnated tablet ceramic, and NZVI/AC, but the cost of MRH is less. More importantly, the uptake amount of MRH is found to be 4.09 mg g^{-1}, equivalent to 40.9 mg of As(V) per gram of iron. It is five times of that of the pure Fe_3O_4 reported by Yean et al. (2005). Furthermore, even though the adsorption capacities of some adsorbents are excellent, their practical application in the arsenate treatment still seems unfeasible and difficult (Dang et al. 2009). Rice husk is a large-capacity agricultural waste in the world, especially in Asia. They should be

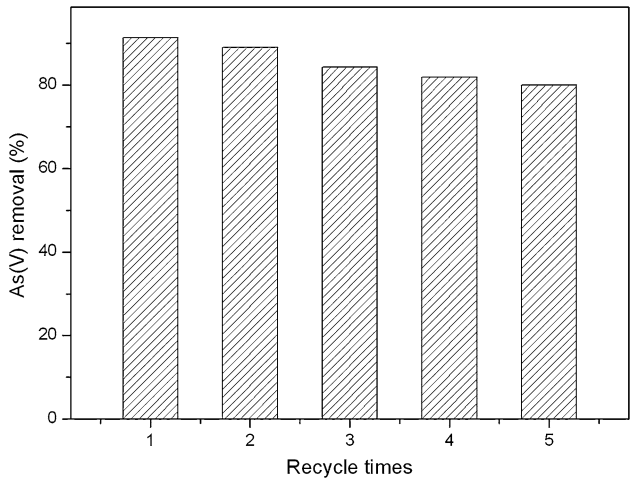

Fig. 8 Removal percentage of As(V) in solutions varied with the number of regeneration cycles. MRH dosage, 2 g L^{-1}; natural pH; agitation rate, 200 rpm; T, 25 ± 2 °C; contact time, 60 min

considered as low-cost, easily available, and synthesized adsorbents applied in environment pollution control. Taking into account of the simple preparation and magnetic separation, the MRH is an effective adsorbent for the removal of As(V) from aqueous solutions.

Regeneration and reuse of MRH

The reusability of adsorbents is important in evaluating their potential for commercial applications. An adsorbent should not only possess high adsorption capability, but also good desorption properties in order to significantly reduce the overall cost of the adsorbent. The MRH was evaluated for deterioration by subjecting to repeated adsorption–desorption using 0.1 M NaOH solution. The adsorption capacities of MRH in consecutive five cycles are shown in Fig. 8. The performance of the MRH slightly deteriorated as the number of regeneration–reuse cycles increased. However, the adsorption efficiency of As(V) could still exceed 80 % after five cycles. This observation indicated that the synthesized MRH was mechanically and chemically stable for As(V) removal from wastewater and source water.

Conclusion

A simple one-step thermochemical method was developed for fabricating MRH composites using cost-effective rice husk. The MRH could adsorb As(V) efficiently and then could be effectively and quickly separated from solutions with an adscititious magnet. Results showed that the adsorption capacity of MRH was higher at neutral media, and it was enhanced with increasing initial concentration of As(V). Three different adsorption kinetic models were employed to assess the adsorption process. It was concluded that the pseudo-second-order kinetics model fitted with adsorption data well and chemical adsorption might be the rate-determining step. Additionally, the fit of the Langmuir adsorption model confirmed the monolayer coverage of As(V) onto the outer space of MRH and also the homogeneous distribution of binding sites on MRH. The adsorption capacity of MRH (4.33 mg g^{-1}) is comparable with several other similar low-cost adsorbents. The MRH were synthesized easily in this study and can be regenerated. The generated data should be useful for designing an economically treatment process for the treatment of As(V)-containing effluents. All the results suggested that the MRH composites can be explored as efficient adsorbents for As(V) treatment in aqueous solutions.

Acknowledgments The authors greatly acknowledge the National Natural Science Foundation of China (No. 41301338), Hunan Provincial Natural Science Foundation of China (No. 13JJ4069), and Scientific Research Staring Foundation for the introduced talents of Hunan Agricultural University (No. 12YJ12).

References

Ai L, Jiang J (2010) Fast removal of organic dyes from aqueous solutions by AC/ferrospinel composite. Desalination 262(1–3):134–140

Bard AJ, Parsons R, Jordan J (1985) Standard potentials in aqueous solutions. Marcel Dekker, New York **162**

Castro MM, Martínez-Escandell M, Molina-Sabio M, Rodríguez-Reinoso F (2010) Hydrogen adsorption on KOH activated carbons from mesophase pitch containing Si, B, Ti or Fe. Carbon 48(3):636–644

Chandra V, Park J, Chun Y, Lee JW, Hwang IC, Kim KS (2010) Water-dispersible magnetite-reduced graphene oxide composites for arsenic removal. ACS Nano 4(7):3979–3986

Chang QG, Lin W, Ying WC (2010) Preparation of iron-impregnated granular activated carbon for arsenic removal from drinking water. J Hazard Mater 184(1–3):515–522

Chen W, Parette R, Zou J, Cannon FS, Dempsey BA (2007) Arsenic removal by iron modified activated carbon. Water Res 41(9):1851–1858

Choi H, Al-Abed SR, Agarwal S, Dionysiou DD (2008) Synthesis of reactive nano-Fe/Pd bimetallic system-impregnated activated carbon for the simultaneous adsorption and dechlorination of PCBs. Chem Mater 20(11):3649–3655

Dang SV, Kawasaki J, Abella LC, Auresenia J, Habaki H, Gaspillo PD, Kosuge H, Doan HT (2009) Removal of arsenic from simulated groundwater by adsorption using iron-modified rice husk carbon. J Water Environ Technol 7(2):43–56

Do MH, Phan NH, Nguyen TD, Pham TTS, Nguyen VK, Vu TTT, Nguyen TKP (2011) Activated carbon/Fe_3O_4 nanoparticle composite: fabrication, methyl orange removal and regeneration by hydrogen peroxide. Chemosphere 85(8):1269–1276

Fang M, Yang L, Chen G, Shi Z, Luo Z, Cen K (2004) Experimental study on rice husk combustion in a circulating fluidized bed. Fuel Process Technol 85(11):1273–1282

Foo KY, Hameed BH (2009) Utilization of biodiesel waste as a renewable resource for activated carbon: application to environmental problems. Renew Sustain Energy Rev 13(9):2495–2504

Freundlich HMF (1906) Über die adsorption in lösungen. Z Phys Chem 57(A):385–470

Ho YS (2006) Second-order kinetic model for the sorption of cadmium onto tree fern: a comparison of linear and non-linear methods. Water Res 40(1):119–125

Ho YS, McKay G (1999) Pseudo-second order model for sorption processes. Process Biochem 34(5):451–465

Jia YF, Xu L, Wang X, Demopoulos GP (2007) Infrared spectroscopic and X-ray diffraction characterization of the nature of adsorbed arsenate on ferrihydrite. Geochim Cosmochim Acta 71(7):1643–1654

Kakavandi B, Jafari AJ, Kalantary RR, Nasseri S, Ameri A, Esrafily A (2013) Synthesis and properties of Fe_3O_4-activated carbon magnetic nanoparticles for removal of aniline from aqueous solution: equilibrium, kinetic and thermodynamic studies. Iranian J Environ Health Sci Eng 10(1):10–19

Kamari A, Wan Ngah WS, Chong MY, Cheah ML (2009) Sorption of acid dyes onto GLA and H_2SO_4 cross-linked chitosan beads. Desalination 249(3):1180–1189

Kannan K, Sundaram MM (2001) Kinetics and mechanism of removal of methylene blue by adsorption on various carbons-a comparative study. Dyes Pigm 51(1):25–40

Lagergren S (1898) Zur théorie der sogenannten adsorption gelöster stoffe. Kungliga Svenska Vetenskapsakademiens. Handlingar 24(4):1–39

Langmuir I (1918) The adsorption of gases on plane surfaces of glass, mica and platinum. J Am Chem Soc 40(9):1361–1403

Liou TH (2004) Evolution of chemistry and morphology during the carbonization and combustion of rice husk. Carbon 42(4):785–794

Liou TH, Wu SJ (2009) Characteristics of microporous/mesoporous carbons prepared from rice husk under base- and acid-treated conditions. J Hazard Mater 171(1–3):693–703

Liu ZG, Zhang FS (2010) Nano-zero valent iron contained porous carbons developed from waste biomass for the adsorption and dechlorination of PCBs. Bioresour Technol 101(7):2562–2564

Liu ZG, Zhang FS, Sasai R (2010) Arsenate removal from water using Fe_3O_4-loaded activated carbon prepared from waste biomass. Chem Eng J 160(1):57–62

Moreno-Castilla C, Carrasco-Marnn F, Mueden A (1997) The creation of acid carbon surfaces by treatment with $(NH_4)_2$-S_2O_8. Carbon 35(10–11):1619–1626

Namduri H, Nasrazadani S (2008) Quantitative analysis of iron oxides using Fourier transform infrared spectrophotometry. Corros Sci 50(9):2493–2497

Oliveira LCA, Pereira E, Guimarae IR, Vallone A, Pereira M, Mesquita JP, Sapag K (2009) Preparation of activated carbons from coffee husks utilizing $FeCl_3$ and $ZnCl_2$ as activating agents. J Hazard Mater 165(1–3):87–94

Patel M, Karera A, Prasanna P (1987) Effect of thermal and chemical treatments on carbon and silica contents in rice husk. J Mater Sci 22(7):2457–2464

Patterson AL (1939) The Scherrer formula for X-ray particle size determination. Phys Rev 56:978–982

Pereira MFR, Soares SF, Orfao JJM, Figueiredo JL (2003) Adsorption of dyes on activated carbons: influence of surface chemical groups. Carbon 41(4):811–821

Sing KSW (1985) Reporting physisorption data for gas/solid systems with special reference to the determination of surface area and porosity (Recommendations 1984). Pure Appl Chem 57(4):603–619

Stuart B, George WO, Mcintyre PS (1996) Modern infrared spectroscopy. John Wiley and Sons, Chichester

Sun HM, Cao LY, Lu LH (2011) Magnetite/reduced graphene oxide nanocomposites: one step solvothermal synthesis and use as a novel platform for removal of dye pollutants. Nano Res 4(6):550–562

Weber WJ, Morris JC (1963) Kinetics of adsorption on carbon from solution. J Sanit Eng Div 89(2):31–60

Yang TZ, Shen CM, Li ZA, Zhang HR, Xiao CW, Chen ST, Xu ZC, Shi DX, Li JQ, Gao HJ (2005) Highly ordered self-assembly with large area of Fe_3O_4 nanoparticles and the magnetic properties. J Phys Chem B 109(49):23233–23236

Yang N, Zhu S, Zhang D, Xu S (2008) Synthesis and properties of magnetic Fe_3O_4-activated carbon nanocomposite particles for dye removal. Mater Lett 62(4–5):645–647

Yean S, Cong L, Yavuz CT, Mayo JT, Yu WW, Kan AT, Colvin VL, Tomson MB (2005) Effect of magnetite particle size on adsorption and desorption of arsenite and arsenate. J Mater Res 20(12):3255–3264

Yun CH, Park YH, Park CR (2001) Effects of pre-carbonization on porosity development of activated carbons from rice straw. Carbon 39(4):559–567

Zanzi R, Bai X, Capdevila P, Björnbom E (2001) Pyrolysis of biomass in presence of steam for preparation of activated carbon, liquid and gaseous products. In: 6th World Congress of Chemical Engineering Melbourne, Australia 23–27

Zhang FS, Itoh H (2005) Iron oxide-loaded slag for arsenic removal from aqueous system. Chemosphere 60(3):319–325

Zhang G, Qu J, Liu H, Cooper AT, Wu R (2007) $CuFe_2O_4$/activated carbon composite: a novel magnetic adsorbent for the removal of acid orange II and catalytic regeneration. Chemosphere 68(6):1058–1066

Zhang F, Li GD, Chen JS (2008) Effects of raw material texture and activation manner on surface area of porous carbons derived from biomass resources. J Colloid Interface Sci 327(1):108–114

Zhang YX, Xu SC, Luo YY, Pan SS, Ding HL, Li GH (2011) Synthesis of mesoporous carbon capsules encapsulated with magnetite nanoparticles and their application in wastewater treatment. J Mater Chem 21:3664–3671

Zhu HY, Fu YQ, Jiang R, Jiang JH, Xiao L, Zeng GM, Zhao SL, Wang Y (2011) Adsorption removal of congo red onto magnetic cellulose/Fe_3O_4/activated carbon composite: equilibrium, kinetic and thermodynamic studies. Chem Eng J 173(2):494–502